Laser linewidth dependence to the transverse mode instability (TMI) nonlinear gain in kW-class fiber amplifiers

Marc D. Mermelstein
MDM Optics, LLC, 320 Raritan Ave. Suite 304A, Highland Park, NJ 08904

ABSTRACT

The thermal grating (TG) and inversion grating (IG) TMI gain dependence on the light beating intensity spectrum is investigated. TMI gain is restricted to intensity bandwidths comparable to the thermal gain bandwidth of ~20 kHz. Seed laser phase noise generates intensity spectra determined by the laser linewidth and the relative modal delay time of the gain fiber. These spectral bandwidths exceed the thermal gain bandwidth by orders of magnitude in both the coherent and incoherent regimes, making them unlikely sources of TMI. It is suggested that phase noise generated in the gain fiber due to external perturbations may be the source of the TMI.

Keywords: fiber amplifiers, transverse mode instabilities

1. INTRODUCTION

Transverse mode instabilities in kW-class fiber amplifiers are primarily understood to originate from the intensity-induced dynamic index gratings in the fiber core [1, 2 and references therein]. There are two kinds of gratings: a thermal grating (TG) and an inversion grating (IG). These gratings or perturbations facilitate the exchange of optical power between the fundamental mode (FM) and a higher order mode (HOM). The analysis presented here assumes that the HOM is seeded by imperfect mode matching at the amplifier launch and that the intensity fluctuation spectra that drive the inversion and consequent gratings is determined by the phase noise of a quasi-monochromatic laser seed source. It is found that bandwidth of the intensity noise in both the coherent and incoherent regimes exceeds the non-linear gain bandwidths associated with the TG an IG by several orders of magnitude. The bandwidth of the TG is determined by a thermal diffusion time constant and is estimated to be ~20 kHz and the bandwidth associated with the IG is determined by the inversion relaxation time and is estimated to be ~0.5 MHz. The large discrepancy in the TMI bandwidth and the driving intensity fluctuation bandwidth indicate that only a small fraction of the total intensity fluctuation power is available to drive the inversion. Therefore it is unlikely that the laser phase noise, characterized by the laser linewidth and the fiber relative modal delay time, is the source of the TMI generation. It is suggested that excess intensity noise generated in the power amplifier with bandwidths comparable to the TMI bandwidth is the source of the TMI.

2. MODELING & ANALYSIS

2.1 Background and problem definition

A ten meter length of commercially available step-index (SI) Yb doped large mode area (LMA) double clad fiber (DCF) is used to model the fiber amplifier [3]. The fiber core has diameter of 25 μm, an inner cladding diameter of 400 μm and a numerical aperture equal to 0.06. (All parameters in the modeling are presented in Table 1 below). It is co-pumped with 975 nm pump laser diodes and a 10 W signal laser at 1083 nm. Numerical simulations indicate that this fiber supports four propagating modes: the LP01, LP02, and LP11 and LP21 modes (calculated with OptiFiber). Experiments show that it is the LP11 HOM that most frequently participates in the power exchange with the LP01 FM. It is initially assumed, for the purposes of analysis, that the each mode conveys monochromatic radiation with optical frequencies and phase constants given by (ω_1, β_1) and (ω_2, β_2) for the FM and HOM respectively. The index gratings originate from a dynamic intensity interference pattern that produces intensity fluctuations at a beat frequency $\Omega=\omega_1-\omega_2$ and a spatial frequency $K=\beta_1-\beta_2$, along with an accompanying modulation in the ion inversion, quantum defect heating, local temperature change and consequent phase-matched and phase-delayed thermal and inversion gratings. Two conditions are required for the power exchange between the FM and HOM: (i) the index grating and the intensity grating must have the same wavevectors equal to K and (ii) there must be a phase lag between the index grating and the intensity grating [4]. The first condition is satisfied by construction and the second condition is satisfied by the relaxation times

Fiber Lasers XV: Technology and Systems, edited by Ingmar Hartl, Adrian L. Carter, Proc. of SPIE
Vol. 10512, 1051221 · © 2018 SPIE · CCC code: 0277-786X/18/$18 · doi: 10.1117/12.2291854

associated with the intensity-to-inversion transduction for the IG and the intensity-to-temperature change transduction for the TG. Two central issues remain somewhat unresolved: (i) what is the source of the initial seeding of the HOM and (ii) what is the source of the frequency difference of the light propagating in each mode? Optical power may be injected into the HOM by distributed elastic Rayleigh scattering due to static inhomogeneities in the core refractive index or due to distributed quasi-elastic Rayleigh scattering arising from thermodynamic temperature fluctuations in the fiber core. Another source of unwanted light injection into the HOM occurs at the fiber input due to an imperfect splice between the power amplifier gain fiber and the preamplifier fiber. Measurements have shown that the unwanted optical power injected into the HOM is approximately 20-30 dB below the optical power injected into the FM [5]. For example, a 10 W FM input power to the fiber amplifier may result in an injection of 10-100 mW into the HOM. Estimates for the total power captured by the HOM from distributed Rayleigh scattering are orders of magnitude smaller. Therefore it is assumed in this analysis that the HOM light originates from an imperfect input splice. In practice, a single quasi-monochromatic laser is used as the light source that illuminates the FM and HOM. In this case, dynamic intensity fluctuations may arise from the self-beating of the light propagating in the FM and HOM and delayed by the fiber relative phase delay time. Hence, the following analysis assumes that the HOM is populated by imperfect mode matching at the amplifier input and that dynamic intensity fluctuations result from the delayed self-homodyne light beating in the LMA gain fiber.

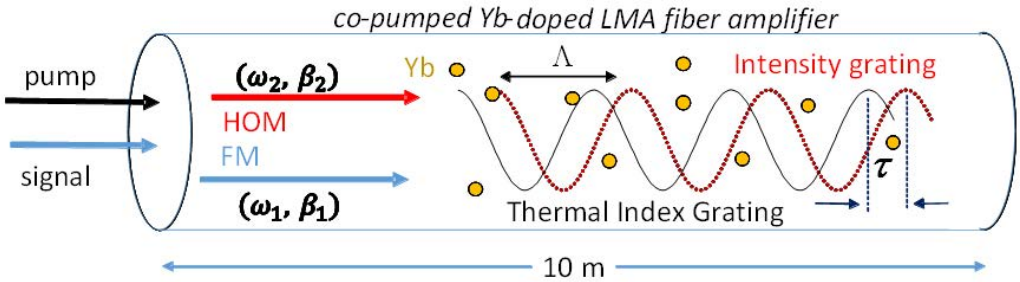

Figure 1. Gain fiber core showing injection of pump and signal power, propagation of FM and HOM at dual frequencies and phase constants, intensity grating and thermal grating.

2.2 Bimodal bichromatic interference pattern

Figure 1 exhibits a section of the gain fiber conveying monochromatic light in the FM and HOM at optical frequencies ω_1 and ω_2, respectively. The electric fields in the fiber at position z and time t are given by:

$$E_1(r,z;t) = A_1(z)\cdot\psi_1(r)\cdot\exp\left\{i\cdot\omega_1\cdot\left[t-t_1(z)\right]\right\} \qquad (1a)$$

$$E_2(r,\varphi,z;t) = A_2(z)\cdot\psi_2(r,\varphi)\cdot\exp\left\{i\cdot\omega_2\cdot\left[t-t_2(z)\right]\right\} \qquad (1b)$$

where $A_{1,2}$ are the complex field amplitudes at position z, $\psi_{1,2}$ are the transverse field distributions , $t_{1,2} = n_e^{(1,2)}\cdot z/c$ are the delay times, $n_e^{(1,2)}$ are the effective modal indices obtained from the numerical simulations based on the fiber refractive index profile and the indices 1 and 2 indicate the FM and the HOM, respectively [6]. The radial coordinate is r, the azimuthal angle is φ, t is time and c is the speed of light in vacuum. The total electric field is given by: $E = E_1 + E_2$. The signal intensity in the fiber $I_S = |E|^2$ is a traveling interference pattern generated by the beating of the FM and HOM. It may be written as: $I_S = \bar{I}_S + \delta I_S$ with a spatially resolved and time averaged pedestal $\bar{I}_S$ and a fluctuating intensity perturbation δI_S are given by:

$$\bar{I}_S(r,\varphi,z) = |A_1(z)|^2\cdot\psi_1^2(r) + |A_2(z)|^2\cdot\psi_2^2(r,\varphi) \qquad (2a)$$

$$\delta I_S(r,\varphi,z;t) = A_1^*(z)\cdot A_2(z)\cdot\psi_1(r)\cdot\psi_2(r,\varphi)\cdot\exp\left\{-i\cdot\left[\Omega\cdot t - K\cdot z\right]\right\} + c.c. \qquad (2b)$$

where c.c. stands for the complex conjugate. This represents a traveling interference pattern with a beat length $\Lambda = 2\pi/K$ where $\beta_{1,2} = n_e^{(1,2)}\cdot k_{1,2}$ are the phase constants, $k_{1,2} = 2\pi/\lambda_{1,2}$ are the wavevectors , $\omega_{1,2} = c\cdot k_{1,2}$ are the

optical frequencies (rad/s) and $\lambda_{1,2}$ are the wavelengths in vacuum. It is assumed that $\delta I_S << \overline{I}_S$ so that the time dependent intensity fluctuations can be treated as a perturbation.

2.3 Ion inversion perturbations, thermal and electronic refractive index modulation

The Yb ions are treated as a two level energy system with a ground state population density of n_1, an excited state population density of n_2 and a ion density $n_0=n_1+n_2$ [7]. Crests in the signal intensity will deplete the excited state population and troughs in the signal intensity will increase the excited state population. The fluctuations in the excited state population density δn_2 may be expressed by expanding n_2 in the signal intensity fluctuations δI_S:

$$\delta n_2(r,\varphi,z;t) = \left(\frac{\partial n_2}{\partial I_S}\right)_0 \cdot \delta I_S(r,\varphi,z;t) \qquad (3)$$

demonstrating that the fluctuations in the excited state population have the same wavevector as the signal intensity fluctuations. Fluctuations in the excited state population will perturb the core refractive index by two mechanisms: the thermo-optic effect and the resonant electronic nonlinearity [8, 9]. In the thermo-optic effect, inversion depletion is accompanied by volumetric heat power generation $\dot{Q}$ due to quantum defect heating. This volumetric heat power creates a local temperature change ΔT with the same wavevector as the intensity fluctuation but with an additional delay time determined by the heat diffusion equation. The heat diffusion equation is solved with a Bessel-Fourier expansion of $\dot{Q}$ and ΔT with time dependent coefficients [10]. The temperature change can be expanded in the intensity fluctuations:

$$\delta T(r,\varphi,z;t) = \left(\frac{\partial T}{\partial \dot{Q}}\right)_0 \cdot \left(\frac{\partial \dot{Q}}{\partial n_2}\right)_0 \cdot \left(\frac{\partial n_2}{\partial I_S}\right)_0 \cdot \delta I_S(r,\varphi,z;t) \qquad (4)$$

where the temperature fluctuations are also proportional to the intensity fluctuations and have a wavevector K.

It is assumed that the heat flow occurs in the radial direction since the core radius a<<Λ. For the LP01 to LP11 transition, the thermal time τ_{1m} constant associated with the m^{th} term of the Bessel-Fourier series is given by:

$$\tau_{1m} = \frac{b^2}{x_{1m}^2 \cdot D} \qquad (5)$$

where x_{1m} is the m^{th} root of the J_1 Bessel function, b is the inner cladding radius, $D = \kappa / \rho \cdot C_P$ is the thermal diffusivity of silica, κ is the thermal conductivity, ρ is the density and C_P is the heat capacity. The index change is proportional to the temperature change with the constant of proportionality equal to the thermo-optic coefficient dn/dT.

The resonant electronic nonlinearity is attributed to the change in electronic polarizability of the Yb ions upon the promotion of an electron from the ground state to the excited state. It is of opposite sign and smaller in magnitude compared to the thermal nonlinearity and enables the transfer of optical power from the HOM to the FM. The spatially resolved inversion relaxation time is given by:

$$\tau_{inv}(r,z) = \frac{1}{\left[\frac{P_1(z)\cdot\psi_1(r)^2}{I_s^{sat}} + \frac{P_P(z)\cdot\psi_P(r)^2}{I_p^{sat}} + \frac{1}{\tau}\right]} \qquad (6)$$

where the pump and signal powers are $P_P(z) = |A_P(z)|^2$, $P_{1,2}(z) = |A_{1,2}(z)|^2$, $P_2(z) << P_1(z)$, τ is the spontaneous emission lifetime, the signal and pump saturation intensities are $I_s^{sat} = h\cdot\omega_S / (\sigma_{as} + \sigma_{es})\cdot\tau$, $I_p^{sat} = h\cdot\omega_P / (\sigma_{ap} + \sigma ep)\cdot\tau$, respectively, σ_{es} (σ_{as}) are the signal emission (absorption) cross sections and σ_{ep} (σ_{ap}) are

the pump emission (absorption) cross sections. A kW amplifier fiber core volume-averaged effective relaxation time $\tau_{eff} = \langle \tau_{inv}(r,z) \rangle$ equal to 1 μs is used here to simplify the analysis.

The evolution of the pump and signal powers are governed by the two level rate equations for the Yb ions [7] and a coupled mode analysis [11] that determines the intensity fluctuation induced power exchange between the FM and the HOM. After a somewhat lengthy analysis that closely follows Refs 7 & 11, the following coupled non-linear power evolution rate equations at a beat frequency Ω are obtained:

$$\frac{dP_P(z)}{dz} = \bar{g}_{PP}(z) \cdot P_p(z) \qquad (7a)$$

$$\frac{dP_1(z)}{dz} = \left[\bar{g}_{11}(z) - \gamma_{12}(z) \cdot P_2(z)\right] \cdot P_1(z) + \left[-\gamma_{th}(z;\Omega) + \gamma_{el}(z;\Omega)\right] \cdot P_1(z) \cdot P_2(z) \qquad (7b)$$

$$\frac{dP_2(z)}{dz} = \left[\gamma_{th}(z;\Omega) - \gamma_{el}(z;\Omega)\right] \cdot P_1(z) \cdot P_2(z) + \left[\bar{g}_{22}(z) - \gamma_{21}(z) \cdot P_1(z)\right] \cdot P_2(z) \qquad (7c)$$

where the time-averaged transversely integrated linear gains are given by:

$$\bar{g}_{PP}(z) = \int_0^{2\pi} d\varphi \int_0^a dr \cdot r \cdot \psi_P^2(r) \cdot \bar{g}_P(r,z) \qquad (8a)$$

$$\bar{g}_{11}(z) = \int_0^{2\pi} d\varphi \int_0^a dr \cdot r \cdot \psi_1^2(r) \cdot \bar{g}_S(r,\varphi,z) \qquad (8b)$$

$$\bar{g}_{22}(z) = \int_0^{2\pi} d\varphi \int_0^a dr \cdot r \cdot \psi_2^2(r,\varphi) \cdot \bar{g}_S(r,\varphi,z) \qquad (8c),$$

the overbar indicates a time averaged value and the normalized pump electric field distribution is $\psi_P = 1/\sqrt{\pi b^2}$ [12].

The signal gain g_S and the pump gain (loss) g_P are given by:

$$g_S(r,\varphi,z;t) = n_2(r,\varphi,z;t) \cdot (\sigma_{es} + \sigma_{as}) - n_0 \cdot \sigma_{as} \qquad (9a)$$

$$g_P(r,\varphi,z;t) = n_2(r,\varphi,z;t) \cdot (\sigma_{ep} + \sigma_{ap}) - n_0 \cdot \sigma_{ap} \qquad (9b).$$

The power evolution Eqs. (7) are solved numerically with a standard Runge-Kutta method. Shown in Figure 2 is the power evolution of the pump, FM and HOM in the absence of nonlinear coupling. Figure 3 shows the linear gain evolutions along the gain fiber.

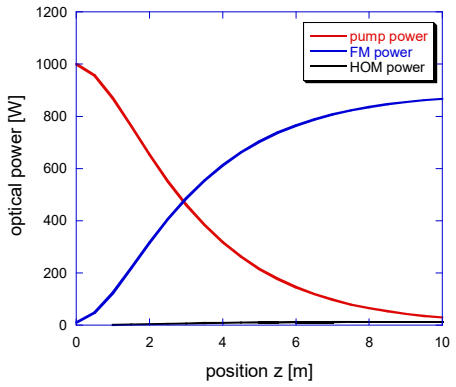

Figure 2. Plot of FM power, HOM power and pump power as a function of position without nonlinear gain. The pump, FM and HOM input powers are: 1000 W, 10 W and 0.1 W, respectively.

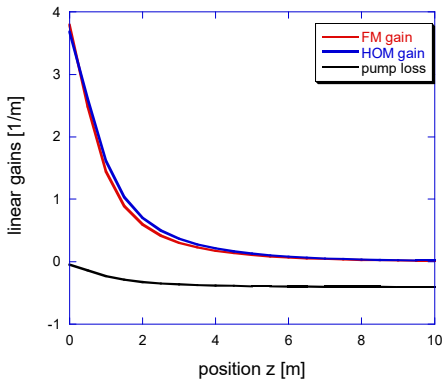

Figure 3. Plot of linear FM, HOM gain and pump loss corresponding to Fig. 2 as a function of position.

The primary non-linearity of interest is the thermo-optic nonlinearity that facilitates the exchange of energy from the FM to the HOM. It is obtained from the transduction of the intensity fluctuations to the temperature fluctuations that generate the phase-matched and phase-delayed thermal index grating. It is given by:

$$\gamma_{th}(z;\Omega) = 2\pi \cdot \frac{dn}{dT} \cdot P_P(z) \cdot \sum_m \frac{I_{1m} \cdot q_{1m}(z) \cdot \Omega \cdot \tau_{1m}}{1+(\Omega \cdot \tau_{1m})^2} \qquad (10a)$$

where

$$I_{1m} = \int_0^a dr \cdot r \cdot \psi_1(r) \cdot J_1\left(\frac{x_{1m} \cdot r}{b}\right) \cdot \psi_2^{(r)}(r) \qquad (10b)$$

and

$$q_{1m}(z) = \int_0^{2\pi} d\varphi \cdot \cos(\varphi) \int_0^a dr \cdot r \cdot \psi_1(r) \cdot J_1\left(\frac{x_{1m} \cdot r}{b}\right) \cdot \psi_2(r,\varphi) \cdot \left[\frac{\bar{n}_2(r,\varphi,z)}{I_{es}} - \frac{\bar{n}_1(r,\varphi,z)}{I_{as}}\right] \qquad (10c)$$

for the LP01 to LP11 transition, where $\psi_2(r,\varphi) = \psi_2^{(r)}(r) \cdot \cos(\varphi)$, $I_{es} = \mathrm{h} \cdot \omega_S / \sigma_{es} \cdot \tau$ ($I_{as} = \mathrm{h} \cdot \omega_P / \sigma_{as} \cdot \tau$) are signal emission (absorption) rate constants and dn/dT is the thermooptic coefficient . Figure 4 shows the two-sided thermal nonlinear gain in the small HOM power limit at fiber positions z=0, 1 & 2 m as a function of beat frequency $\Omega/2\pi$. The maximum gain appears at the amplifier input with a value of 0.14 1/m-W at a beat frequency of 6 kHz and falls to a maximum value of 0.016 1/m-W at z=2 m. The gain bandwidth is approximately 20 kHz.

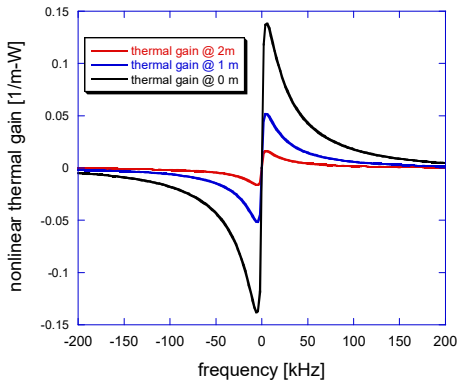

Figure 4. Plot of nonlinear thermal gain as a function of beat frequency at fiber positions z=0, 1 and 2 m for co-pumped amplifier.

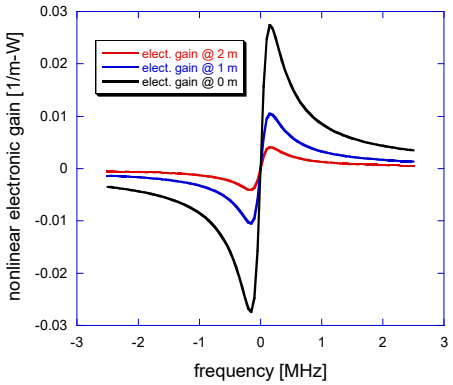

Figure 5. Plot of resonant electronic nonlinear gain as a function of beat frequency at fiber positions z=0, 1 and 2 m for co-pumped amplifier.

The resonant electronic nonlinearity is given by:

$$\gamma_{el}(z;\Omega) = \frac{4\pi \cdot k_0 \cdot \Delta n_r \cdot f(z)}{n_0} \cdot \frac{(\tau_{eff}/\tau) \cdot (\Omega \cdot \tau_{eff})}{1+(\Omega \cdot \tau_{eff})^2} \qquad (11a)$$

where

$$f(z) = \int_0^{2\pi} d\varphi \int_0^a dr \cdot r \cdot \psi_1(r)^2 \cdot \psi_2(r,\varphi)^2 \cdot \left[\frac{\bar{n}_2(r,\varphi,z)}{I_{es}} - \frac{\bar{n}_1(r,\varphi,z)}{I_{as}}\right] \qquad (11b)$$

and $\Delta n_r \cong 7x10^{-7}$ [8] is the estimated core index change for 100% inversion of the Yb dopant at 1083 nm. Figure 5 shows the electronic resonant gain as a function of beat frequency. The maximum gain is 0.027 1/m-W at z=0 m at a beat frequency of 150 kHz and falls to a maximum gain of 0.004 1/m-W at z=2 m. The gain bandwidth is approximately 0.5 MHz.

Nonlinear gains γ_{12} and γ_{21} represent intermodal gain depletion between the FM and HOM at a beat frequency Ω .The presence of optical power in the HOM robs gain that would otherwise be available to the FM, thereby reducing the FM gain. Similarly, the FM uses gain that would otherwise be available to the HOM. These nonlinear gains are given by:

$$\gamma_{12}(z;\Omega) = \gamma_{21}(z;\Omega) = (\sigma_{es} + \sigma_{as}) \cdot f(z) \cdot \frac{(\tau_{eff}/\tau)}{1 + (\Omega \cdot \tau_{eff})^2} \qquad (12)$$

Shown in Figure 6 is a plot of the gain depletion nonlinearity as a function of beat frequency. Note that the gain depletion is much less than the thermal nonlinear gain so the net nonlinear gain will be approximated by:

$$\gamma(z;\Omega) = \gamma_{th}(z;\Omega) - \gamma_{el}(z;\Omega) \qquad (13)$$

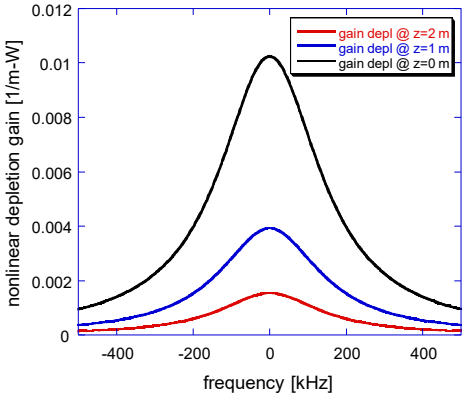

Figure 6. Plot of gain depletion nonlinearity γ_{12} As a function of beat frequency at fiber positions Z=0, 1 and 2 m for copumped amplifier

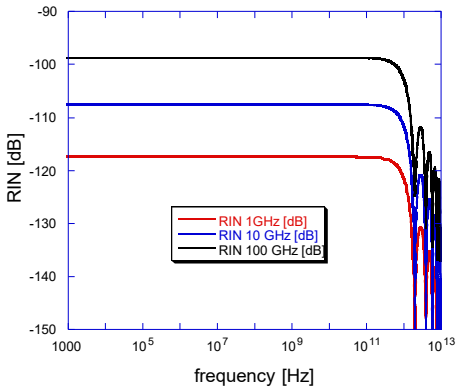

Figure 7. Plot of calculated RIN spectrum for coherent mixing of FM and HOM light at z=0.5 m for laser linewidths of 1, 10 and 100 GHz. Fiber relative phase delay time per unit length is ~1 ps/m.

2.4 Delayed self-homodyne intensity spectrum

In the above analysis a fictitious bimodal bichromatic light source was used to illuminate the LMA gain fiber and populate the FM and HOM with optical frequencies ω_1 and ω_2 respectively. This was done as an analytic method to calculate the nonlinear gain coefficients as a function intensity fluctuations at a beat frequency Ω. In practice, the fiber is illuminated with a quasi-monochromatic laser source with a central frequency ω_0, full-width at half-maximum (FWHM) of $\Delta\omega_{1/2}$ and a coherence time $\tau_c = 2/\Delta\omega_{1/2}$. In this case the nonlinear gain is driven by a spectrum of intensity fluctuations. The electric fields in the fiber at position z and time t are given by:

$$E_1(r,z;t) = A_1(z) \cdot \psi_1(r) \cdot \exp\left\{i \cdot \omega_0 \cdot \left[t - t_1(z)\right] + i \cdot \varphi\left[t - t_1(z)\right]\right\} \qquad (14a)$$

$$E_2(r,\varphi,z;t) = A_2(z) \cdot \psi_2(r,\varphi) \cdot \exp\left\{i \cdot \omega_0 \cdot \left[t - t_2(z) + i \cdot \varphi\left[t - t_2(z)\right]\right]\right\} \qquad (14b)$$

where $\varphi(t)$ is the stochastic phase fluctuations of the quasi-monochromatic laser. The fluctuating intensity perturbation is now given by:

$$\delta I_S(r,\varphi,z;t) = A_1^*(z)\cdot A_2(z)\cdot\psi_1(r)\cdot\psi_2(r,\varphi)\cdot\exp\left\{i\cdot\left[K\cdot z+\Delta\varphi(t,\tau)\right]\right\}+c.c. \qquad (15)$$

where $K=\Delta n_e\cdot k_0$, $\Delta n_e = n_e^{(1)}-n_e^{(2)}$ is the differential modal index , $\omega_0 = c\cdot k_0$, $k_0 = 2\pi/\lambda_0$, λ_0 is the central wavelength of the quasi-monochromatic light source, $\tau(z)=t_1(z)-t_2(z)$ is the differential time delay and the phase jitter is: $\Delta\varphi(t,\tau)=\varphi(t)-\varphi(t+\tau)$ where the phase fluctuations are assumed to be stationary. This represents a dynamic intensity interference pattern with wavevector K and phase jitter $\Delta\varphi(t,\tau)$. Numerical simulations indicate that the FM and HOM exhibit a relative phase delay per unit length of ~1 ps/m. Intensity fluctuations in the core will result from beating of the two modes. Coherent mixing of the light in the two modes over the entire length of the gain fiber can be assured for laser linewidths less than ~64 GHz (or $\Delta\lambda$ = 25 nm). Plotted in Figure 7 are the relative intensity noise (RIN) spectra for coherent mixing at laser linewidths of 1, 10 and 100 GHz for a relative delay time Δt of 0.5 ps corresponding to position z=0.5 m in the gain fiber [13,14]. The RIN calculation is done at the quadrature positions where the conversion from phase fluctuations to intensity fluctuations is the greatest. It is seen that the RIN spectra are nearly flat out to the first minimum given by Δt^{-1} and that the bandwidth exceeds that of the thermal nonlinear gain by many orders of magnitude. This will be true for the entire length of the fiber, i.e. the RIN spectra will be flat and broad banded. Hence, the greater portion of the intensity fluctuation power is not available to the nonlinear gain. Also, the RIN level increases with increasing laser linewidth, yet experimental results indicate that the TMI threshold is independent of laser linewidth [15]. One can define an effective net nonlinear gain by integrating the bimodal bichromatic net nonlinear gain over the normalized intensity fluctuation power spectrum $S(z;\Omega)$ for the quasi-monochromatic source:

$$\gamma_{eff}(z) = \frac{\int_0^\infty d\Omega\cdot\gamma(z;\Omega)\cdot S(z;\Omega)}{\int_0^\infty d\Omega\cdot S(z;\Omega)} \qquad (16)$$

This approach yields an effective net nonlinear gain nearly equal to zero due the very large mismatch in gain-bandwidths. Hence, it is unlikely that the delayed self-homodyne intensity noise in can act as a driver for the TMI generation.

2.5 Amplifier excess phase and intensity noise

Section 2.5 investigated the phase and intensity noise in the MOPA that originates in the seed laser. Experiments employing a Mach-Zehnder interferometer with the fiber amplifier in one arm of the interferometer and a single mode fiber in the reference arm of the interferometer have shown that an excess phase noise is generated in the amplifier [16, 17]. This phase noise relative to the reference arm is attributed to perturbations acting upon the gain fiber. They include temperature variations, mechanical resonances, acoustic noise and pump power noise. The power spectra of the phase and intensity noise qualitatively exhibit a $1/f^{\alpha}$ frequency dependence where the index $1\le\alpha\le 2$ and the spectra are restricted to a bandwidth of approximately 100 kHz. It is assumed that a LMA gain fiber subjected to the same perturbations will exhibit a similar relative phase noise between the FM and HOM. A normalized phenomenological intensity noise spectra for the excess amplifier intensity noise may be described by:

$$S(\omega)\sim\begin{cases}\dfrac{A}{\omega} & \omega_0<\omega<\omega_C\\[2ex] \dfrac{A\cdot\omega_C}{\omega^2} & \omega_C<\omega<\infty\end{cases} \qquad (17)$$

where A is a constant, ω_0 is a low frequency limit taken to be 100 Hz and ω_C is a corner frequency demarking the transition from a $1/\omega$ spectral frequency dependence to a $1/\omega^2$ frequency dependence. Shown in Figure 8 is a plot of

the normalized amplifier intensity noise spectra (in arbitrary units) as a function of frequencies between 100 Hz and 1.0 MHz for corner frequencies of 100 Hz, 1 kHz and 10 kHz. Substitution of the intensity noise spectra Eq. (17) into Eq. (16) yields plots of the effective net TMI gain $\gamma_{eff}(z)$ as a function of fiber position z. These are shown in Figure 9. It is seen that the overlap of the phenomenological excess amplifier noise spectrum with the TMI gain spectrum yields a significant net effective nonlinear gain and

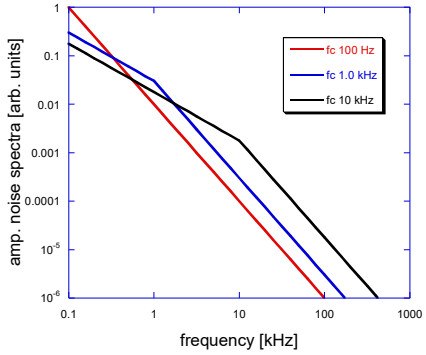

Figure 8. Plot of phenomenological amplifier intensity noise spectra with corner frequencies of 100 Hz, 1 kHz and 10 kHz.

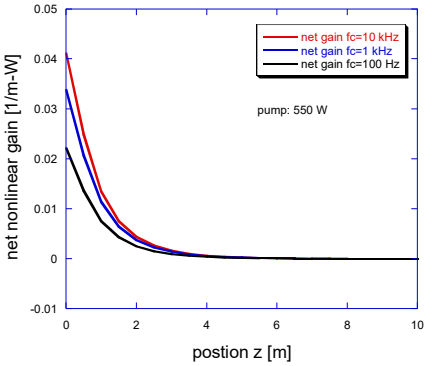

Figure 9. Plot of effective net gain as a function of fiber position for three intensity noise spectra shown in Figure 8.

that the more rapidly decreasing intensity spectra leads to a lower effective TMI gain. The spectrally weighted effective TMI gains are used in the coupled rate equations (7) to calculate the pump and signal power evolutions. Figure 10 shows the optical powers as a function of fiber position with the effective nonlinear gains given by Eqs (10-17). The model demonstrates the transfer of approximately 10% of the FM to the HOM for the $1/f^2$ excess amplifier intensity noise spectra. The threshold powers for the three spectra are demonstrated in Figure 11 which plots the HOM power vs. the FM power. The threshold powers range from 400-500 W.

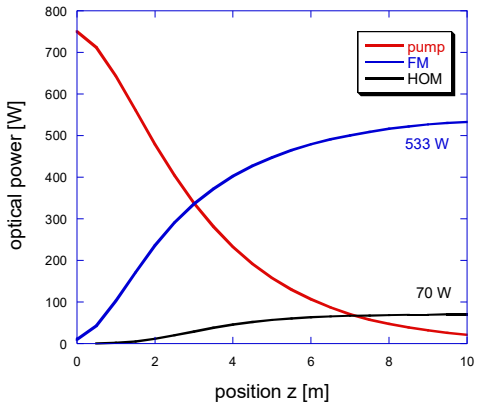

Figure 10. Plot of pump, FM and HOM power evolution as a function of fiber position with TMI nonlinearities. TG mode coupling transfers optical power from the FM to the HOM. Approximately 12% of the total signal power appears in the HOM.

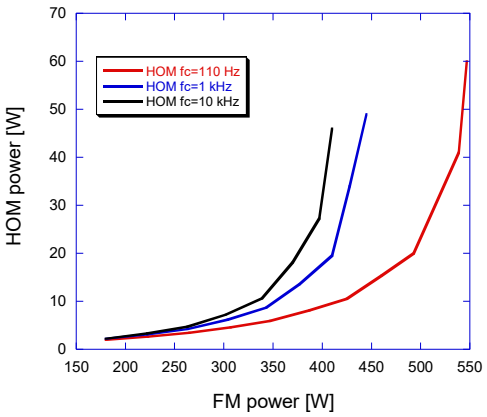

Figure 11. Plot of the HOM power vs. the FM power for the excess amplifier intensity noise spectra shown in Fig. 8. A threshold power of 500 W is estimated for the $1/f^2$ excess amplifier intensity noise.

3. CONCLUSION

A coupled mode formalism combined with an Yb two level energy model has been utilized to quantitatively characterize the exchange of optical power between the FM and HOM in a LMA Yb-doped kW-class fiber amplifier. The coupled pump, FM and HOM power evolution rate equations enable the calculation of the TMI threshold power as a function of fiber and amplifier characteristics. It is assumed that the HOM is seeded by imperfect mode matching at the amplifier input. Modal interference in the gain fiber generates an intensity perturbation that modulates the core refractive index and generates mode coupling index gratings. The thermo-optic index grating (TG) enables power transfer from the FM to the HOM and the resonant electronic or inversion grating (IG) enables power transfer from the HOM to the FM. It is found that the TG exhibits a peak gain of 0.14 1/m-W at 6 kHz with a bandwidth of 20 kHz and that the IG exhibits a peak gain of 0.03 1/m-W at 150 kHz with a bandwidth of 0.5 MHz. It is initially assumed that coherent delayed self-homodyne intensity fluctuations drive the grating formation. However, the bandwidth of these intensity fluctuations exceeds that of the TG nonlinear gain by several orders of magnitude suggesting that only a small fraction of the intensity fluctuation power is available to drive the inversion modulation. Also the magnitude of the intensity fluctuations is expected to scale with the laser linewidth, yet experiments show that the TMI threshold is independent of laser linewidth. Therefore, it is suggested that perturbations applied to the gain fiber generate an excess amplifier intensity noise with a bandwidth comparable to the TG gain bandwidth thereby generating the TMI. This transduction mechanism requires more rigorous theoretical examination and experimental corroboration.

Table 1.

Fiber parameters		
Inner core radius	a	12.5 μm
Inner cladding radius	b	200 μm
Inner core numerical aperture	NA	0.06
LP01 effective index	$n_e^{(1)}$	1.4528635
LP11 effective index	$n_e^{(2)}$	1.4525010
Relative phase delay	$\Delta\tau$	1.2 ps/m
Signal wavelength	λ_S	1083 nm
Pump wavelength	λ_P	975 nm
Beat length	Λ	3.0 mm
Thermal conductivity	κ	1.38 W/m-deg
density	ρ	2200 kg/m^3
Heat capacity	C_P	700 J/kg-deg
Thermal Diffusivity	D	$8.96x10^{-7}$ m^2/s
Thermo-optic coefficient	dn/dT	$1.1x10^{-5}$ deg^{-1}
Gain medium parameters		
Yb ion density	n_0	$4.1x10^{25}$ m^{-3}
Pump emission cross section	σ_{ep}	$2.58x10^{-24}$ m^2
Pump absorption cross section	σ_{ap}	$2.58x10^{-24}$ m^2
signal emission cross section	σ_{es}	$2.30x10^{-25}$ m^2

Signal absorption cross section	σ_{as}	$1.69x10^{-27}$ m^2
Spontaneous emission lifetime	τ	0.84 ms
effective inversion lifetime	τ_{eff}	1.0 μs
Electronic index change	Δn_r	$7x10^{-7}$
Planck's constant	h	$1.05x10^{-34}\ J-s$

REFERENCES

[1] Zervas, M. N., "Transverse mode instability analysis in fibre amplifiers," Proc. SPIE 10083, 100830M (2017).
[2] Jauregui, C., Limpert, J. and Tunnermann, A.," High power fiber lasers," Nat. Photonics 7 (11), 861-867 (2013).
[3] Nufern Fiber LMA-YDF-25/4-VIII; www.nufern.com
[4] Silberberg, Y. Bar-Joseph, I, "Optical instabilities in nonlinear Kerr medium," J. Opt. Soc. Am. B 1, 662 (1984).
[5] Nicholson, J.W., Yablon, A.D., Ramachandran, S. and Ghalmi, S., "Spatially and spectrally resolved imaging of modal content in large-mode-area fibers," Opt. Express 16 (10), 7233-7243 (2008).
[6] Neumann, E.-G., [Single-Mode Fibers], Springer-Verlag, Berlin (1988).
[7] Becker, P.C., Olsson, N.A. and Simpson, J.R., [Erbium-doped Fiber Amplifiers], Academic Press, San Diego (1999).
[8] Arkwright, J.W., Elango, P., Atkins, G.R., Whitbread, T. and Digonnet, M.J.F., "Experimental and theoretical analysis of the resonant non-linearity in Ytterbium-doped fiber," J. Lightwave Technol., 16, 798 (1998).
[9] Fotiadi, A., Antipov, O., Kuznetsov, M. and Megret, P., "Refractive index changes in rare earth-doped optical fibers and their applications in all-fiber coherent beam combining," in [Coherent Laser Beam Combining], Wiley, Weinheim (2013).
[10] Jackson, J.D., [Classical Electrodynamics], John Wiley & Sons, Inc., New York (1962).
[11] Yariv, A. and Yen, P., [Optical Waves in Crystals], John Wiley & Sons, Inc., Hoboken (2003).
[12] Jiang, Z. and Marciante, J. R. "Impact of transverse spatial-hole burning on beam quality in large-mode-area Yb-doped fibers," J. Opt. Soc. Am. B 25, 247 (2008).
[13] Gallion, P. B., and Debarge, G. "Quantum phase noise and field correlations in single frequency semiconductor laser systems," IEEE J. of Quant. Electron., QE-20, 343 (1984).
[14] Tkach, R.W. and Chraplyvy, A.R., "Phase noise and linewidth in InGaAsP DFB lasesr," J. Lightwave Techn. LT-4, 1711 (1986).
[15] Ward, B., Robin, C. and Dajani, I., "Origin of thermal modal instabilities in large mode area fiber amplfiers," Opt. Express 20 (10), 11407 (2012).
[16] Augst, S. J., Fan, T. Y. and Sanchez, A. "Coherent beam combining and phase noise measurements of ytterbium fiber amplifiers," Opt. Letts., 29, 474 (2004).
[17] Trobs, M., Wessels, P., and Fallnich, "Power-and frequency-noise characteristics of an Yb-doped fiber amplifier and actuators for stabilization," Opt. Express 13 (6), 2224-2235 (2005).